Molecular Study of Ultrasound-Triggered Release of Fluorescein from Liposomes

Fatima El Hajj, Patrick F. J. Fuchs, Wladimir Urbach, Mohammad Nassereddine, Salah Hamieh, Nicolas Taulier

Molecular study of ultrasound-triggered release of fluorescein from liposomes

Fatima El Hajj,[†,‡] Patrick F. J. Fuchs,[¶] Wladimir Urbach,[§] Mohammad Nassereddine,[‡] Salah Hamieh,[‡] and Nicolas Taulier[*,†]

†*Sorbonne Université, CNRS, INSERM, Laboratoire d'Imagerie Biomédicale, LIB, F-75006 Paris, France*

‡*Faculté des Sciences, Université Libanaise, Liban*

¶*Université de Paris*

§*Laboratoire de Physique de l'École Normale Supérieure, ENS, Université PSL, CNRS, Sorbonne Université, Université de Paris, F-75005 Paris, France.*

E-mail: nicolas.taulier@sorbonne-universite.fr

Abstract

Several investigations have suggested that ultrasound triggers the release of drugs encapsulated into liposomes at acoustic pressures low enough to avoid cavitation or high hyperthermia. However, the mechanism leading to this triggered release as well as the adequate composition of the liposome membrane remain unknown. Here, we investigate the ultrasound triggered release of fluorescein disodium salt encapsulated into liposomes made of 1,2-dioleoyl-sn-glycero-3-phosphocholi (DOPC) or 1,2-distearoylphosphatidyl-ethanolamie (DSPC) lipids with various concentrations of cholesterol (from 0 to 44 mol%). The passive release of encapsulated fluorescein was first characterized. It was observed to be higher when the membrane is in a fluid phase and increased with temperature but decreased upon addition of cholesterol. Next, the release of fluorescein was measured at

different acoustic frequencies (0.8, 1.1, 3.3 MHz) and peak-to-peak pressures (0, 2, 2.5, 5, 8 MPa). Measurements were performed at temperatures where DOPC and DSPC liposomes were respectively in the fluid or gel phase. We found that the release rate did not depend on the ultrasound frequency. For DOPC liposomes, the ultrasound-triggered release of fluorescein decreased with increasing concentration of cholesterol in liposomes, while the behavior was more complex for DSPC liposomes. Overall, the triggered release from DSPC liposomes was up to ten times less than DOPC liposomes. Molecular dynamics simulations performed on a pure DOPC membrane showed that a membrane experiences, under a directional pressure of ±2.4 MPa, various changes in properties such as the area per lipid (APL). An increase in APL was notably observed when the simulation box was laterally stretched or perpendicularly compressed, which was accompanied by an increase in the number of water molecules crossing the membrane. This suggests that ultrasound most probably enhances the diffusion of encapsulated molecules at small acoustic pressures by increasing the distance between lipids.

Introduction

Most liposomes are non-toxic, biodegradable, and spherical objects whose diameters range from 50 nm to 100 µm. They are composed of one or several phospholipid bilayers separating an inner aqueous volume from the outer aqueous environment. This gives them the ability to serve as a storage compartment for active agents of different lipophilicities.[1] Thanks to these properties, liposomes are considered as a primary choice to be used as drug carriers.[1] For such medical applications, unilamellar liposomes with a diameter around 100 nm are usually considered. Nowadays, most drug carriers that have been clinically approved are liposomal formulations such as caelyx (i.e. doxorubucin encapsulated inside liposomes).[2] Even if current commercial liposomal systems only offer a non-controlled drug release, they still succeed in improving the drug efficiency by increasing the drug dose at the site of diseased tissue

after intravenous injection, most probably thanks to the enhanced permeation and retention (EPR) effect. It is also possible to target liposomes to specific receptors[3] and even control the drug delivery using various external (e.g. electric, magnetic or ultrasonic) stimuli.[4] So far, the only liposomal system under clinical trial that has been developed for such control is thermodox,[5] that is a liposomal formulation of doxorubicin which is thermosensitive, to the contrary of caelyx. The thermosensitivity is due to the existence of a gel-to-liquid transition in the lipid membrane at a critical temperature T_m which depends on the lipid characteristics. In the gel phase (below T_m), the lipid membrane is impermeable while it becomes permeable in the liquid phase (above T_m). To use this mechanism, one simply needs to slightly increase the local temperature using an appropriate external stimulus as well as the appropriate lipid composition. However, it is difficult to induce a mild hyperthermia only on a small and precisely localized area due to heat dissipation. The use of focused ultrasound offers other mechanisms on top of hyperthermia with a high degree of spatial localization. The advantage of ultrasound is that it is already widely used in clinics for diagnostic purposes and its therapeutic use is growing. The release mechanism depends on the acoustic parameters such as frequency f, acoustic pressure P, duty cycle (DC), pulse repetition frequency (PRF), and insonation duration τ. Acoustic pressure is a key parameter, as it dictates the occurrence of cavitation (appearance and implosion of bubbles from dissolved gases) at a specific frequency. Cavitation is a violent event that can induce many bio-effects such as cell sonoporation, creation of free radicals, protein denaturation, hemorrhage and burns.[6] Ultrasound-induced cavitation can be used to trigger the release of drugs encapsulated into liposomes, by rupturing the lipid membrane, but this approach implies that all bioeffects due to cavitation are occuring in the whole insonified region, including adverse effects. To avoid these effects , many investigations have focused on using ultrasound to induce mild hyperthermia in combination with the use of thermosensitive liposomes. In this approach, small to moderate acoustic pressures (of hundreds of kPa to several MPa) are used, which avoids the occurrence of cavitation. Still, as mentioned earlier a precise localization of the

drug delivery is lost due to heat dissipation.

However, Oerlemans et al.[7] showed that it was possible to release a drug encapsulated into non-thermosensitive liposomes without having to rely on heat or cavitation, but instead using a mechanism that still needs to be precised. Indeed, the authors used ultrasound to trigger an important release of fluorescein encapsulated into DSPC/cholesterol/PEG_{2000}-DSPE. Meanwhile, they showed that no fluorescein release was achieved upon heating, up to 60℃, and that inertial cavitation induced by the addition of hexafluoride microbubbles during insonation did not enhanced fluorescein release. Previously, Evjen et al.[8,9] also demonstrated the possibility to release drugs from non-thermosensitive liposomes using ultrasound. However no action has been made by the authors to detect cavitation, although the low pressure used was in favor of the absence of cavitation. Interestingly, the authors showed that a significantly larger ultrasound-triggered release of doxorubicin was achieved when using liposomes made of either 1,2-Distearoyl-sn-glycero-3-phosphoethanolamine (DSPE)[8] or DOPC[9] rather than DSPC, the other ingredients being DSPC-PEG and cholesterol. Giustetto et al.[10] succeeded to trigger the release of a magnetic resonance imaging agent (Gadoteridol) encapsulated into liposomes by applying low intensity, non-focused, pulse or continuous ultrasound. They validated the approach on mice and their histology results suggested the absence of inertial cavitation. In a more recent work, Novell et al.[11] observed an increase in the release of calcein encapsulated into non-thermonsensitive liposomes when using long insonation (>10 min). Finally, Mujoo et al.[12] showed that the addition of bile salt to the liposome membrane (made of 1,2-dioleoyl-sn-glycero-3-phosphoethanol amine (DOPE), DSPC, and cholesterol) reduced the release of encapsulated carboxyfluorescence. In their investigation, the absence of cavitation was demonstrated using an assay for hydroxyl radicals and a temperature elevation of 2℃ was measured at the transducer focus.

All these investigations show that ultrasound can be used to trigger the delivery of drugs encapsulated into liposomes without having to induce inertial cavitation or to use thermosensitive liposomes, but the understanding of the underlying mechanism is still unclear. The

aim of this article is to gain a better understanding of this release mechanism. We used fluorescein as a model drug to evaluate its release from the variation in fluorescence intensity as a function of lipid saturation, cholesterol concentration and acoustic properties (below the inertial cavitation threshold). DOPC (di18:1 PC) and DSPC (di18:0 PC) lipids were chosen as they are well studied and often used for many applications such as a model membrane or as a drug carrier. Finally, to obtain a molecular view of the effects of a compression or a stretching on the lipid membrane properties, molecular dynamics simulations were performed on a DOPC membrane, since the largest amount of released fluorescein was experimentally achieved under insonation for DOPC liposomes devoid of cholesterol.

Materials and Methods

Materials

Solutions of 1,2-dioleoyl-sn-glycero-3-phosphocholine (di18:1 PC or DOPC) and 1,2-distearoylphosphatidyl-ethanolamine (di18:0 PC or DSPC) were purchased from Avanti Polar Lipids as solubilized in chloroform. Cholesterol, phosphate buffer and Triton-X100 were purchased from Sigma-Aldrich, and fluorescein disodium salt (technical grade) was purchased from VWR. The cholesterol assay kit was obtained from Cayman Chemical and the lipid quantification kit was from Cell Biolabs, Inc. Water was purified using a PURELAB Option-Q unit (from ELGA LabWater).

Liposomes preparation

Liposomes were prepared by the thin film hydration method.[13] 0, 0.75, 1.5 or 2.25 mg of cholesterol were added to 200 µL of a solution containing 25 mg/mL of either DOPC or DSPC dissolved in chloroform. By doing so, the cholesterol:lipid composition in mol% were estimated to be [0:100], [23:77], [38:62], and [48:52]. The four compositions were prepared for DSPC liposomes while only the first three were prepared for DOPC. Next, the lipid

mixtures were rotary evaporated under vacuum until they were dry. The resulting lipid films were hydrated with 0.5 mL of a solution containing a high concentration of sodium fluorescein (80 mg/mL) dissolved in a phosphate buffer solution (PBS) (pH = 7.4). The fluorescein concentration was chosen to ensure its quenching. The resulting lipid dispersions were sonicated at 40 W for 5 min with pause cycles of 30 s, and then extruded using a polycarbonate membrane with a pore size of 200 nm (Avanti, PC membrane 0.2 µm). In order to remove the unencapsulated sodium fluorescein, the liposomes suspensions were filtered using a microcentrifugal filter tube (ThermoFisher, Pierce™ Protein Concentrator), containing an ultrafiltration membrane of 100 kDa. This filter retained the liposomes while letting the solvent, solubilizing unencapsulated fluorescein, to go through it. Before filling the microcentrifugal filter tubes, the samples were diluted 4 times with PBS. Then, the tubes were centrifuged at 12,000 g for 1 h 30 min, thus reducing the volume of the liposome solution to 50 µL. The filtered solution was removed then the liposome solution was diluted and filtered again. This process was repeated 4 times to make sure that no free sodium fluorescein remained.

Cholesterol-to-lipid ratio

We used two specific commercial kits to separately determine the amount of cholesterol and of lipids for each of our liposome formulation in the absence of fluorescein. The cholesterol assay kit (from Cayman Chemical) is based on an enzyme-coupled reaction. In this kit, cholesterol is first oxidized by cholesterol oxidase to yield hydrogen peroxide and the corresponding ketone product. In the presence of horseradish peroxidase, hydrogen peroxide reacts with 10-acetyl-3,7-dihydroxyphenoxazine in a 1:1 stoichiometry to produce highly fluorescent resorufin. The lipid quantification assay kit (from Cell Biolabs, Inc) measures the neutral lipid content using a lipid binding molecule that only fluoresces when it is bound to lipids.

The enzymatic reaction and the binding of the fluorescent molecules were restricted in

the case of saturated lipids.[14] Thus, the addition of 10% of Triton X-100 to the suspension followed by heating at 60℃ (i.e. above the temperature of transition) for 1 h 30 min was necessary to enhance the accessibility of the enzymes and the fluorescent molecules. Next, liposomes were cooled down at room temperature and diluted 10× or 800× in water for lipid or cholesterol assay, respectively, so that the final concentration of Triton-X was respectively 1% and 0.0125%. The resulting fluorescence intensity of both the lipid and the cholesterol assay was recorded at an emission wavelength of 595 nm using an excitation wavelength of 485 nm, at which the contribution of Triton-X was negligible. Both the cholesterol and lipid amounts were derived from a comparison with a reference curve measured from standard solutions.

Size measurement

The average hydrodynamic diameter D size along with the Polydispersity Index (PDI) of liposomes in suspension were measured by dynamic light scattering (DLS). Measurements were performed with an ALV/CGS-3 platform based goniometer system (from ALV GmbH) at 25℃, at scattering angles ranging from 50° to 130° with a step of 20°. At each angle θ, the device provided the decay rate Γ_θ whose values were plotted as a function of the scattering vector amplitude $q(\theta) = \frac{4\pi n}{\lambda} \sin(\theta/2)$, where $n = 1.333$ is the refractive index of the solution and $\lambda = 633\,\text{nm}$ is the laser wavelength. For each sample, the values of D and PDI were obtained from a fit of the curve using the cumulant method.[15]

Fluorescein release

The passive or ultrasound-triggered release of fluorescein was determined by fluorescence spectroscopy using a JASCO spectrofluorometer (model FP 8300). The fluorescence signal coming from the fluorescein encapsulated into the liposomes is quenched due to the high concentration of encapsulated fluorescein. Since all free fluorescein has been previously removed during liposome preparation, any release of fluorescein will be accompanied by an

increase in the fluorescence signal. Thus, in these measurements, we first measured the fluorescent spectra F_0 of the liposome solution before incubation or insonation. The fluorescence intensity in this spectra is low because of the quenching of encapsulated fluorescein, but was not null due to a passive release occurring between the time of liposome preparation and experiments. After an incubation or insonation lasting an amount of time t, the fluorescence spectra $F(t)$ was measured again. At this stage, surfactant Triton X-100 was added to the liposome solution at a concentration of 1%. The surfactant permeabilized the lipid membrane, leading to the release and dilution of all fluorescein. The fluorescent spectra F_{lyz} of this solution reflects a signal characteristic of the total amount of fluorescein. Consequently, the percentage R of released fluorescein was derived using the equation:

$$R = \frac{F_t - F_0}{F_{lyz} - F_0} \times 100 \tag{1}$$

Fluorescein load in liposomes

The quantity of encapsulated fluorescein M_{enc} is the difference between the total amount of added fluorescein during sample preparation M_{tot} and the amount M_{free} of fluorescein that was not encapsulated after liposome formation. The total amount of added fluorescein was known by weighing it and is equal to $M_{tot} = 40\,\mu g$ ($= 80\,\mu g/mL \times 0.5\,mL$). After liposome formation, the amount of unencapsulated sodium fluorescein was evaluated from the volume V of the filtered solution going through the first ultrafiltration. The filtered solution was diluted 2000× in PBS (pH 7.4) and its fluorescence intensity was measured from 500 to 550 nm using a JASCO spectrofluorometer (model FP 8300) at an excitation wavelength of 494 nm. The concentration C_{free} of free fluorescein was determined using the fluorescence intensity at 515 nm and a calibration curve previously measured from solutions solubilizing free sodium fluorescein, with a fluorescein concentration ranging from 0.007 to 31.25 µg/mL. The amount of free fluorescein is the amount of fluorescein contained in the filtered solution $M_{free} = C_{free}V$.

Ultrasonic setup

The experiments dealing with insonation were performed using an in-house set-up built specifically for this purpose (Fig. 1). It consisted of a waveform generator (model 33220A from Agilent) that generated an electric signal that was amplified by a radio frequency amplifier (model 150A100C from AR France). Before being converted into an acoustic signal by a focused transducer (model H-101-G from Sonic Concepts), a wattmeter (model NRT from Rhode & Schwarz) continuously monitored the average power. The focused transducer was placed vertically inside a water bath connected to a water degassing and heating unit (model WDS-1005 from Sonic concepts) adjusted at a temperature of 22 or 37°C. A cylinder whose diameter was adjusted to the transducer diameter held a sample holder. The cylinder wall contained holes allowing temperature homogenization between the inside and outside volumes. The cell holder was made of a disk where the sample occupied the center. The sample volume (of 1000 mm^3) was separated from the bath water by a thin plastic film. An ultrasound absorbing material was located one centimeter above the sample holder to avoid ultrasound reflection. We used ultrasonic signals at three frequencies: 0.8, 1.1, or 3.3 MHz. The focus was located partly inside the sample volume and the location was identical between experiments made at the same frequency owed to the set-up design. The focus volume located inside the sample volume differed according to the frequency: its value was 41.75 mm^3 at 0.8 MHz, 17.44 mm^3 at 1.1 MHz, and 0.87 mm^3 at 3.3 MHz (taken at -6 dB). Ultrasound was emitted during 20 min at a duty cycle of 5% and a pulse repetition frequency of 200 Hz. This means that the signal was a repetition pulses made of 200, 275, and 825 sinusoidal cycles when the frequency was respectively 0.8, 1.1, and 3.3 MHz. Finally, the acoustic pressure at the ultrasound focus was measured using a 0.5 mm needle hydrophone (working from 0.1 to 40 MHz with an error lower than 10% in the frequency range used here) from Precision Acoustics in the absence of samples and plastic film.

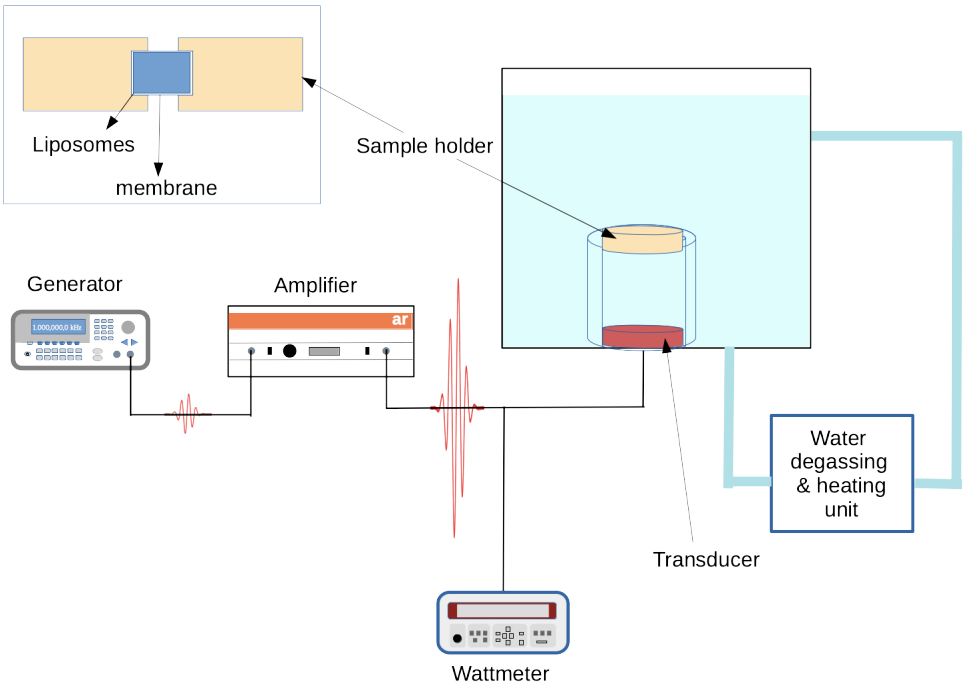

Figure 1: Schema of the ultrasonic setup.

Cavitation dosimetry

The terephthalate dosimeter is a sensitive technique to detect the occurrence of inertial cavitation when insonation lasts more than a minute,[16] such as in our experiments. Briefly, cavitation creates reactive oxygen species such as hydroxyl radicals $^{\bullet}$OH and hydrogen radicals H$^{\bullet}$. Hydroxyl radicals will bind the non-fluorescent terephthalate (TA) to form the fluorescent hydroxyl-terephthalate (HTA). Consequently, the fluorescence intensity will increase as the number of HTA is formed. While in the absence of cavitation, no radicals will be produced and the fluorescent intensity will not vary. Thus, the quantity of generated HTA is proportional to the cavitation dose.[17,18]

In our measurements, 2 mM of TA was prepared in phosphate buffer and maintained at pH 7.3. It is known that the HTA fluorescence signal is linearly proportional to the HTA concentration in the range of 0.2–20 µM. The number of HTA generated under insonation was generally lower than 20 µM in the literature.[19,20] As a fluorescence reference, we used a

HTA solution prepared with the same buffer at a concentration of 1 µM. The fluorescence intensities, F and F_0 , of the TA solution was measured, at an excitation wavelength of 315 nm and emission wavelength of 422 nm, respectively before and after insonation. The concentration of HTA created due to the occurrence of inertial cavitation is derived from the equation:

$$C_{\mathrm{HTA}} = \frac{F - F_0}{F_{ref}} \times C_{ref} \tag{2}$$

where C_{HTA} is the concentration of generated HTA and F_{ref} is the fluorescence of the reference HTA solution containing a HTA concentration of $C_{ref} = 1\,\mu\mathrm{M}$.

Experimental design

Seven liposome formulations encapsulating sodium fluorescein were prepared either from saturated lipid DSPC mixed with cholesterol at mole fraction of 0, 23, 38, and 48 mol%, or unsaturated lipid DOPC mixed with Cholesterol: 0, 23, and 38 mol%. We determined the liposome hydrodynamic size, the amount of encapsulated sodium fluorescein and the effective [cholesterol:lipid] mole fractions or all of the seven formulations. We also studied the passive and ultrasound-triggered release of fluorescein at various acoustic pressures and frequencies. For all experiments, the measurements were performed in triplicate.

Statistics

Statistics were performed using python 3.8.1 and scipy 1.6.0. All fits were performed using the least-square method and were evaluated using the chi-square goodness of fit test (or one-way chi-square test). Tests for linear correlation were performed by calculating the Pearson correlation coefficient. In addition, p-value was derived to test the non-correlation. Comparisons of the mean values between two groups were performed using a two-samples T-test, after verifying that each data group followed a normal distribution (using the Shapiro-Wilk test) with an equal variance (using the Levene test).

Molecular dynamics simulations

Two systems consisting of a pure DOPC membrane of different size were constructed using the CHARMM-GUI[21] webserver: a small one of 100 DOPC (50 per leaflet) and a large one of 1024 DOPC (512 per leaflet). Both were fully hydrated (40 molecules of water per lipid), but without ions. As usual, the bilayer was located on the *xy* dimension of the box, while the *z* dimension corresponded to the normal to the membrane. The different procedures described below were applied to both systems. We first used the CHARMM-GUI procedure which starts by a minimization followed by a thermalization. Then, an equilibration was performed using position restraints on the lipids which were progressively released. At the end of this, we got a starting structure before proceeding to the different simulations. We performed 5 different simulations. The first one was a control simulation at 0.1 MPa in both *xy* and *z* dimensions. So far, two main strategies were followed in the literature for simulating the effect of an acoustic pressure. The first one mimics the effect of a shockwave by setting initial velocities in the shockwave direction.[22] This approach does not model the ultrasound wave per se but the effect of its dissipation. It has been used mainly to study the consequence of cavitation. The second strategy is to translate the acoustic wave into a pressure applied to the system.[23] Since we wanted to study the effect of modest acoustic intensities applied for long times, we chose the second strategy which better describes the physics at play.

Accordingly, in the four other simulations, we applied a pressure of ± 2.4 MPa on the box either on the *xy* or *z* dimension (see Table 1). It is important to note that when we applied a positive pressure, it could be seen as a compression of the simulation box, whereas for a negative pressure it could be seen as a stretching of the box. Since the membrane was in the *xy* plane, we used the word *lateral* when we applied a pressure there, whereas we used the word *perpendicular* when we applied a pressure on the *z* dimension. For the four simulations under ± 2.4 MPa pressure, 1 ns of equilibration was performed. We then proceeded to the production run (500 ns for the small bilayers, 30 ns for the large ones).

Table 1: List of simulations.

acronym	pressure xy (MPa)	pressure z (MPa)	description
0.1MPa-xyz	+0.1	+0.1	control
0.1MPa-xy_2.4MPa-z	+0.1	+2.4	perpendicular compression
0.1MPa-xy_-2.4MPa-z	+0.1	−2.4	perpendicular stretching
2.4MPa-xy_0.1MPa-z	+2.4	+0.1	lateral compression
-2.4MPa-xy_0.1MPa-z	−2.4	+0.1	lateral stretching

The CHARMM36 force field[24] was used throughout this study. All molecular dynamics simulations were carried out using GROMACS version 2018.5[25] within the NPT ensemble. The systems were equilibrated with the Berendsen thermostat[26] at 295.15 K (with a time constant of 1 ps; lipids and water coupled separately) and the Berendsen barostat at the wanted pressure with a time constant of 1 ps and a compressibility of $4.5 \times 10^{10}\,\mathrm{Pa}^{-1}$. Production simulations were run at 295.15 K using the velocity-rescaling thermostat[27] with a time constant of 1 ps (lipids and water coupled separately) and at the wanted pressure using the Parrinello-Rahman barostat[28] with a time constant of 5 ps and a compressibility of $4.5 \times 10^{10}\,\mathrm{Pa}^{-1}$. Pressure coupling was applied semi-isotropically: the scaling of the x and y dimensions were coupled, whereas the z direction was scaled independently from x and y. The bond lengths were constrained using the P-LINCS algorithm.[29] A time step of 2 fs was used with the leapfrog integrator. The water molecules were kept rigid using the SETTLE algorithm.[30] Lennard-Jones interactions were computed using a force-switching function[31] over 1.0 to 1.2 nm. The smooth particle-mesh Ewald method[32,33] was used for computing electrostatic interactions with a real space cutoff of 1.2 nm. Frames were saved every 10 ps (100 ps for the large membranes of 1024 lipids) for subsequent analysis. All of the molecular graphics were generated with VMD.[34] For all of the simulation analysis, we systematically removed the first 10 ns of simulation to extract equilibrium properties (area per lipid, membrane thickness, and lipid order parameter). We analyzed the small patch trajectories in order to extract the area per lipid (APL), the membrane thickness and order parameter. For all equilibrium properties, the uncertainty was evaluated by block averaging. Each trajec-

tory was divided into 5 blocks and the reported uncertainty is the standard deviation of the means of each block. For the order parameter, it is not reported since it was systematically below 0.02 as reported in some other study.[35] The APL was calculated as the xy box area divided by the number of lipids per monolayer. Membrane thickness was calculated using a density plot from the distance between the two crossovers. The order parameter S_{CD} of each C-H bond was calculated using:

$$S_{CD} = \frac{1}{2}\langle 3\cos^2(\theta) - 1\rangle \tag{3}$$

where θ is the angle between the C-H bond and the membrane normal (z axis), and $\langle ...\rangle$ means ensemble averaging. The script *fluxer.py*[36] was used for monitoring water permeation through the membrane (downloaded from `http://www.cgmartini.nl` on october 2020).

Results

Liposomes properties

We prepared liposomes made of either DSPC or DOPC with various concentrations of cholesterol. All of these liposome formulations were prepared so that liposomes encapsulate sodium fluorescein. The fluorescein concentration inside a liposome (around 80 mg/mL at the beginning of the preparation) was large enough to induce its fluorescence quenching. The liposome solution was washed so that only negligible free fluorescein was present. We measured liposome mean diameters from DLS that were significantly different ($p = 0.0015$) between liposomes made of DSPC or DOPC, while the mean diameter did not depend significantly on the concentration of cholesterol. The mean diameters were 175 ± 10 nm and 145 ± 10 nm, (with PDI of 0.34 ± 0.17 and 0.41 ± 0.07) for liposomes made, respectively, of DSPC and DOPC. In our experiments, we used solutions diluted four times where the concentration of encapsulated sodium fluorescein was about 4.0 ± 0.2 mg/mL for all liposome formulations.

For each formulation, the amounts of cholesterol and lipid added to the solution led to the following composition ([mol% cholesterol:mol% lipids]): [0:100], [23:77], [38:62], and [48:52]. Since a loss of materials can be expected after filtration and centrifugation, we derived the composition at the end of the liposome preparation, by separately measuring the quantity of lipids and of cholesterol using specific kits. The error produced by the cholesterol kit was less than 1% and less than 0.1% for the lipid kit. The effective compositions were then [20:80], [33:67], and [44:56] for the last three formulations of DSPC liposomes, and [22:78] and [34:66] for the second and third formulation of DOPC liposomes.

Passive fluorescein release

We monitored the passive release for each liposome formulation. To do so, we measured the difference in fluorescence intensity at a time t, then 20 min later. For DOPC formulations, 20 min incubations were performed at 22, 26, 30, 34, 38, 42, 46 and 50°C, knowing that $T_m < 0$ for a DOPC membrane. The percentage of released fluorescein R was plotted as a function of temperature for DOPC liposomes containing 0, 22 and 34% of cholesterol, represented respectively by blue, red and green circles in the top figure of Fig. 2. For each formulation, the release increased as the temperature rised, but the addition of cholesterol reduced the amount of released fluorescein. The data was well fitted by the following equation (using the least square minimization method):

$$R(T) = AT + BT^2 \tag{4}$$

where A and B were constants with no physical significance.

For DSPC formulations, higher temperatures were investigated as we knew that the critical temperature of the gel-to-liquid phase transition was around 54.5°C for liposomes made of only DSPC.[37] Thus, measurements were performed at 22, 38, 42, 46, 50, 54, 58, and 62°C. The data is displayed at the bottom figure of Fig. 2 for DSPC liposomes containing

0, 20, 33, and 44% of cholesterol (in blue, red, green, and black squares, respectively). The fluorescein release was small below a critical temperature T_m, then abruptly increased to reach a plateau above T_m, the value of which decreased as the percentage of cholesterol increased. The R value at 22℃ was below 0.1% for all liposome formulations. The data was fitted using an equation taking into account a transition at a critical temperature T_m:[38]

$$R(T) = AT + BT^2 + \frac{\Delta R}{1 + e^{(T_m - T)}} \tag{5}$$

where ΔR was the release due to the gel-to-liquid transition. From the fit of the experimental data, we derived ΔR and T_m for DSPC liposomes containing respectively 0, 20, 33, and 44 mol% of cholesterol. For ΔR, these values were respectively, (92 ± 10), (91 ± 3), (17 ± 3) and (1.8±1.5)%, while the values of T_m were respectively (51.3±0.5), (45.9±0.3), (42.4±0.5), and (54.6 ± 2.5)℃ (see inset plot in Fig. 2).

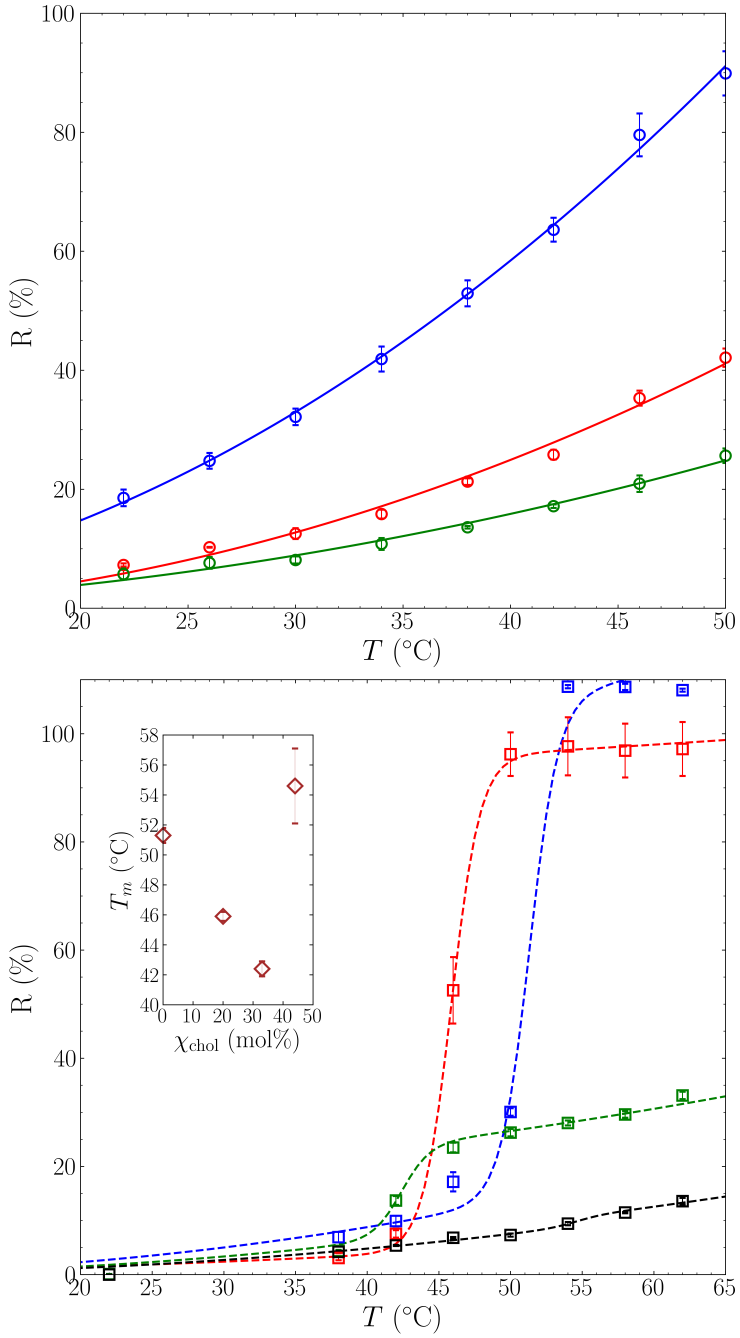

Figure 2: Percentage of released fluorescein as a function of temperature when using liposomes made of either DOPC (top figure) with 0 mol% (○), 22 mol% (○), 34 mol% (○) of cholesterol or DSPC (bottom figure) with 0 mol% (□), 20 mol% (□), 33 mol% (□) or 44 mol% (□) of cholesterol. The lines represent fits by Eq. 4 for DOPC and Eq. 5 for DSPC. The chi-square analysis gave the following p-values for DOPC : $p = 0.999$ (–), 0.996 (–), 0.999 (–) and for DSPC: $p = 0.554$ (---), 0.950 (---), 0.959 (---) and 981 (---). The inset plot displays the T_m values derived from the fit as a function of the cholesterol mole fraction into the liposome membrane.

Ultrasound-triggered release of fluorescein

The ultrasound-triggered release experiments were performed at 22 and 37℃ for liposomes containing DOPC and at 37℃ for DSPC liposomes. The temperature 37℃ was chosen because of its physiological relevance. Since the passive release was important ($> 40\%$) for DOPC liposomes at 37℃, we also decided to investigate a lower temperature where the passive release was smaller ($< 20\%$), that is 22℃, the lower temperature previously explored. Experiments were performed as previously explained, except that an insonation was performed during 20 min instead of a 20 min incubation. For all insonations, the pulse repetition frequency was set to 200 Hz while the duty cycle was kept equal to 5%, *i.e.* a pulse of 0.25 ms was emitted every 5 ms during the 20 min of insonation. This also means that at each pulse emission, ultrasound was "on" during the first 5% of the time (i.e. during $t_{\text{on}} = 0.25\,\text{ms}$) and "off" during the remaining 95% (i.e. during $t_{\text{off}} = 4.75\,\text{ms}$). The first experiments were performed at an acoustic frequency of 1.1 MHz, which was the fundamental frequency of the transducer used in our setup. Each liposome sample was insonified at different acoustic peak-to-peak pressures: 0, 2, 2.5 and 5 MPa. These pressures were determined in the absence of liposomes using a needle hydrophone. The data for DOPC liposomes is displayed in the top figure of Fig. 3. The insonation enhanced the fluorescein release when liposomes were devoid of cholesterol, at 22 and 37℃, or when they contained 22 mol% of cholesterol at 37℃. For the other conditions, i.e at 22 mol% of cholesterol at 22℃ and at 34 mol% of cholesterol at 22 and 37℃, the release enhancement was small. The data for DSPC liposomes is displayed in the top figure of Fig. 4. For all of the conditions except at $\chi_{\text{chol}} = 20\%$ for DSPC and $\chi_{\text{chol}} = 0\%$ for DOPC at 37℃, a positive correlation was significantly observed between fluorescein release R and pressure P_{pkpk}.

Next, we investigated the ultrasound-triggered release of encapsulated fluorescein at three frequencies (0.8, 1.1, and 3.3 MHz) as shown in the bottom figures of Fig. 3 and 4 for DOPC and DSPC liposomes respectively. In these figures, we considered ΔR, the pressure-normalized difference in the fluorescein release before and after insonation, since the peak-

to-peak pressure was 2 MPa at 1.1 and 3.3 MHz, but 8 MPa at 0.8 MHz. However, we did not normalize these values by the insonified volume despite the fact that this volume decreases as the frequency increases. Indeed, we considered that a 20 min insonation allowed the insonation of all liposomes in the sample volume thanks to diffusion and convection. This assumption was confirmed by the fact that we could measure values of 100% for fluorescein release. To make sure that no inertial cavitation occured, particularly at the lower frequency, we assessed its occurrence using a teraphtalate dosimetry (data not shown). No increase in HTA production was observed (< 0.008 µM) at the three frequencies, which confirmed that inertial cavitation did not occur during our measurements. For liposomes made of DOPC, the percentage of fluorescein release per MPa, ΔR, decreased as the cholesterol fraction in the liposomes increases. Similar ΔR values were obtained at 1.1 and 3.3 MHz while they were smaller at 0.8 MHz. These values confirmed that the insonified volume was not relevant otherwise ΔR would have dramatically decreased. The best values were obtained for liposomes devoid of cholesterol or containing 22 mol% of cholesterol when $T = 37$℃. For DSPC liposomes, ΔR were much smaller as they never exceeded 1.5% during the 20 min of insonation. Surprisingly, negative values were obtained at 20 mol% of cholesterol. During all of the insonation experiments, only small temperature elevations were measured: that were 0, 0.3, and 1.8℃ at $f = 1.1$ MHz for $P_{pkpk} = 2$, 2.5 and 5 MPa, respectively, 0.5℃ at $f = 3.3$ MHz and $P_{pkpk} = 0.5$ MPa, and 2.1℃ at $f = 0.8$ MHz and $P_{pkpk} = 8$ MPa. The heat maps in Fig. 6S, 7S, 8S and 9S display the two-samples T-test between all points displayed in each figure.

In conclusion, These results showed that the amount of fluorescein release triggered by ultrasound depends on: (i) the lipid membrane phase (the release is the most important for the liquid crystalline phase, in absence of cholesterol, and it decreases for increasing cholesterol concentration in the liquid disordered phase), (ii) the peak-to-peak pressure (a significant positive correlation is obtained for most configurations), (iii) frequency only for DOPC liposomes (as shown by the heatmap of Fig. 7S and 9S).

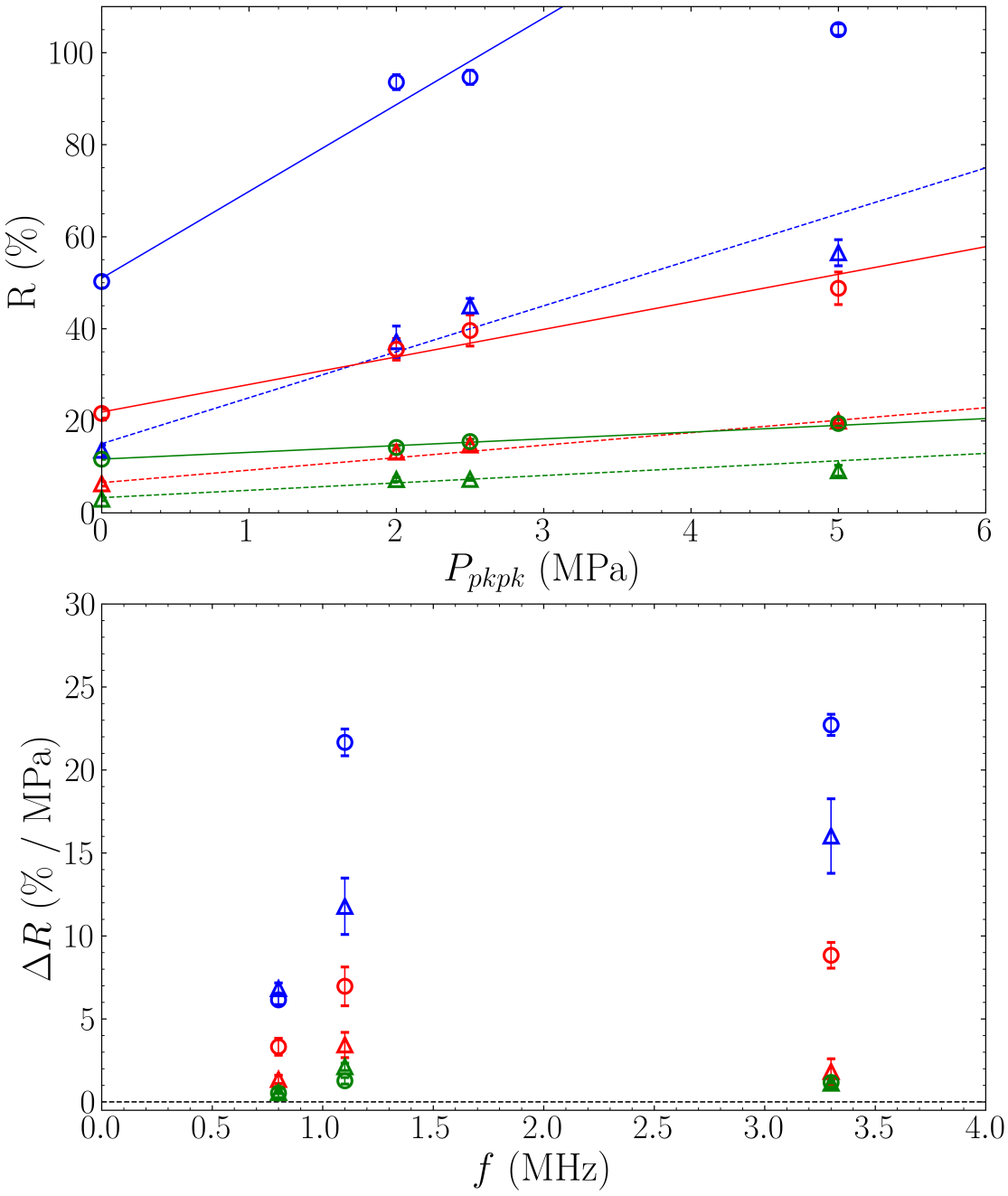

Figure 3: Top figure: Percentage of released fluorescein as a function of acoustic peak-to-peak pressure using liposomes made of DOPC at 22℃ (△, △, △) and 37℃ (○, ○, ○) with 0 mol% (△, ○), 22 mol% (△, ○), and 34 mol% (△, ○) of cholesterol. The lines are linear fit of the data, for which a chi-square analysis gave the following p-values, at 22℃: $p = 0.576$ (---), 0.963 (---), 0.915 (---), at 37℃: $p = 0.816$ (–), 0.925 (–), 0.999 (–). The Pearson correlation coefficients between R and P_{pkpk} are respectively at 22℃: 0.96 (---, $p = 0.037$), 0.98 (---, $p = 0.012$), 0.94 (---, $p = 0.059$), at 37℃: 0.88 (–, $p = 0.113$), 0.98 (–, $p = 0.019$), 0.99 (–, $p = 0.003$). Bottom figure: Enhancement of fluorescein release, per unit of acoustic pressure, due to ultrasound triggering at frequencies of 0.8, 1.1 and 3.3 MHz.

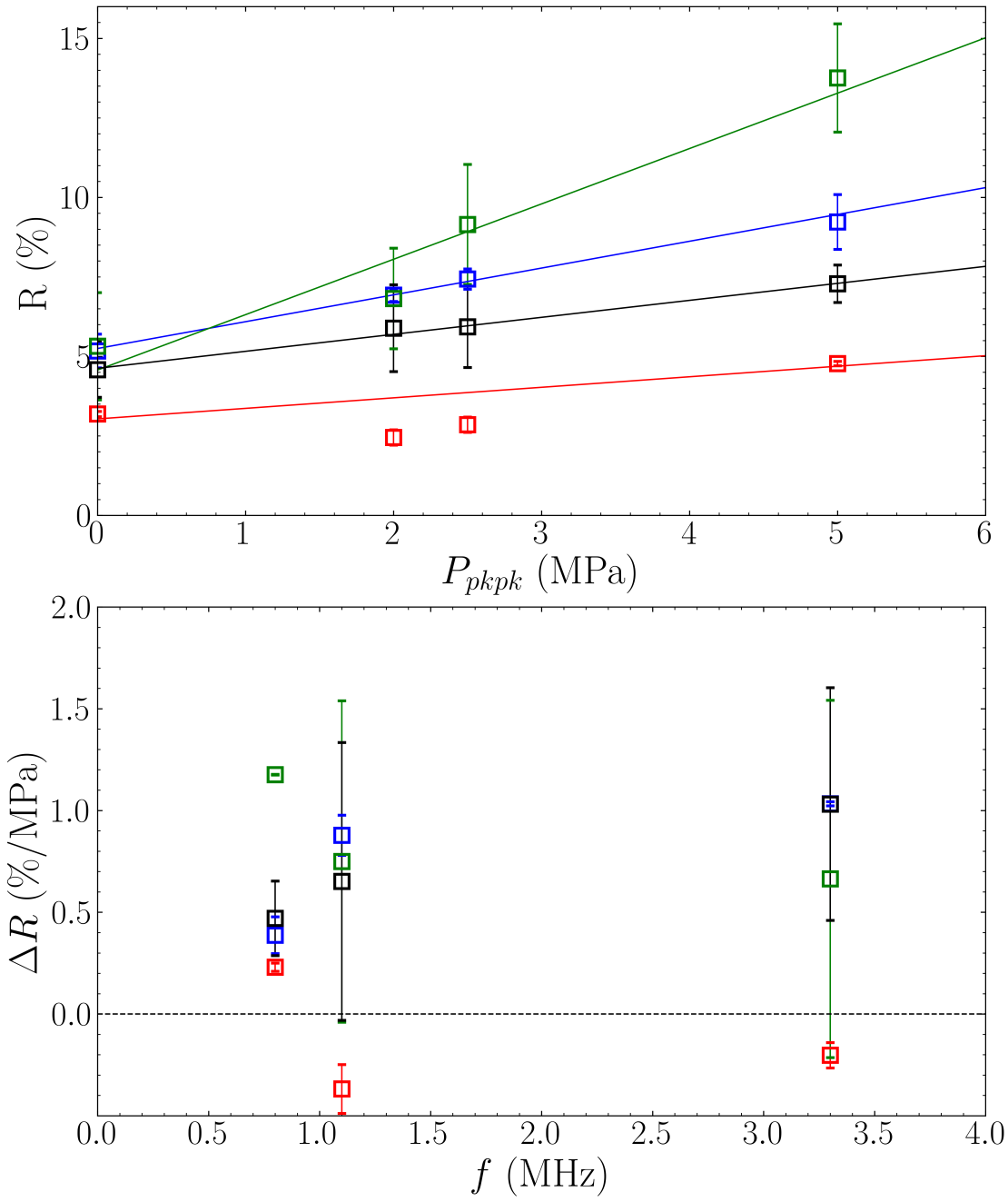

Figure 4: Top figure: Percentage of released fluorescein as a function of acoustic peak-to-peak pressure using liposomes made of DSPC at 37°C with 0 mol% (□), 20 mol% (□), 33 mol% (□) or 44 mol% (□) of cholesterol. The lines are a linear fit of the data. A chi-square analysis gave the following p-values: $p = 0.999$ (–), 0.875 (–), 0.953 (–), and 0.999 (–). The Pearson correlation coefficients between R and P_{pkpk} are respectively: 0.99 (–, $p = 0.002$), 0.70 (–, $p = 0.299$), 0.97 (–, $p = 0.029$), 0.99 (–, $p = 0.005$). Bottom figure: Enhancement of fluorescein release, per unit of acoustic pressure, due to ultrasound triggering at frequencies of 0.8, 1.1 and 3.3 MHz.

Molecular dynamics simulations

To obtain molecular insights on the effect of pressure on a phospholipid membrane, we performed molecular dynamics (MD) simulations on DOPC bilayers. We chose a lipid composition devoid of cholesterol as the effect of acoustic pressure on fluorescein release was the most dramatic. Because we were primarily interested in molecular details such as water permeation, we chose an all-atom representation. Accordingly, we could not consider a whole liposome but simulated a box containing squared membrane patches of modest size: a small one of 100 lipids ($\sim 25\,\mathrm{nm}^2$) and a larger one containing 1024 lipids ($\sim 441\,\mathrm{nm}^2$). For both sizes, periodic boundary conditions were applied in all dimensions as routinely used in the field. For this reason, it is important to bear in mind that finite size effects may appear. Moreover, we did not simulate the whole sinusoidal variation of an acoustic pressure $P(t)$ as it was not yet implemented in recent GROMACS versions. Instead, we applied either a positive (compression) or negative (stretching) pressure of 2.4 MPa on the box along the xy or z dimension, the membrane being located along the xy plane. This value of 2.4 MPa would represent the maximum acoustic pressure of a sinusoidal wave having a peak-to-peak pressure of about 4.8 MPa. Since only membrane patches were simulated, we consider two specific cases where the pressure was applied to the box either perpendicularly or parallel to the membrane plane (i.e. along xy). We also performed control simulations where the box was under a uniform pressure of 0.1 MPa in all directions. Small patches of 100 DOPC lipids were simulated to obtain a "local" information, mainly at the lipid level. Whereas the larger patches of 1024 lipids were simulated to assess larger deformations such as membrane bending. A list of the different simulations performed in this work is shown in Table 1.

From the small size simulations, we first derived the order parameters S_{CD} for each C-H bond of the polar head (top panel of Fig. 5) and the fatty acyl chains (bottom panel of Fig. 5 and Fig. 1S) of all DOPC lipids. In general, an increase of order parameter (i.e. when it goes away from 0, thus when -S_{CD} increases for most of the C-H bonds) means that the lipids are more packed against each other. In contrast, a decrease means the lipids are less packed and

thus freer to move around. The labels used in Fig. 5 correspond to DOPC atoms as given in Fig. 2S. The black symbols correspond to the control membrane that is under a pressure of 0.1 MPa in all directions. Under lateral pressures (i.e. along xy) of ± 2.4 MPa, the DOPC order parameters S_{CD} increased for a laterally compressed membrane (i.e. $+2.4$ MPa), while S_{CD} decreased for a laterally stretched membrane (i.e. -2.4 MPa). Under a perpendicular pressure (i.e. along z) of ± 2.4 MPa, a perpendicularly compressed membrane reduced the DOPC order parameters S_{CD}, while a perpendicularly stretched membrane increased S_{CD}. These effects were observed on all C-H bonds of the two acyl chains. However, most of the C-H bonds in the polar head were not or poorly affected by the applied pressures. Only, g3_1, g2_1 and g1_1 presented a change of order parameter similar to that of the acyl chains.

We also derived the area per lipid (APL) a and the membrane thickness d, which are displayed in Table 2 (see also Fig. 3S and 4S for the corresponding barplots). The control membrane exhibited an APL of 67.5 Å^2 and a membrane thickness of 42.5 Å (first row in Table 2). A perpendicular compression of the membrane induced both an increase in the APL (by 4.4 Å^2) and a diminution of the membrane thickness (by 3.1 Å) compared to the control membrane (second row in Table 2). A perpendicular stretching induced opposite effects: a decreased by 4.3 Å^2, while d increased by 1.7 Å (third row in Table 2). On the other hand, a parallel compression led to a decrease of 4.0 Å^2 in a value and an increase of 1.9 Å in d value compared to the control membrane (fourth row in Table 2) and a parallel stretching led to an increase in a value of 4.8 Å^2 and a decrease in d value of 1.5 Å (fifth row in Table 2).

All these results in terms of order parameter, APL and membrane thickness were perfectly consistent and led to the following intuitive observations: the effect of a perpendicular compression (magenta) of the box was similar to a lateral stretching (red), while the effect of a perpendicular stretching (green) was similar to a lateral compression (blue).

We further derived the number of hydrogen bonds N_{hb} between the water molecules and

DOPC polar heads (see Fig. 6). This number logically increased from 740 to 757–758 upon a rise in APL, while it decreased from 740 to 721–722 when the APL was reduced as mentioned in Table 2 (see also Fig. 5S for the corresponding barplots).

Next, we determined the number of water molecules crossing the DOPC membrane as a function of time. We observed that under a directionnal pressure of ±2.4 MPa there was more water crossing the DOPC bilayer than at a uniform pressure of 0.1 MPa, except when the membrane was perpendicularly stretched.

We studied larger size membranes in order to monitor effects that could not be visualized on small membranes due to finite size effects. Fig. 7 displays the variation of the lateral size of the simulation box along with the final conformation of the membrane after 30 ns of simulation. We observed that the membrane area, which is directly proportional to the lateral box size (as shown in Fig. 7), expanded when a compression was applied perpendicularly to the membrane plane (magenta line) or when a stretching was applied parallel to the membrane plane (red line). These results were in agreement with the small membrane simulations (APL and order parameter increased, thickness decreased). In contrast, membrane buckling was observed under a perpendicular stretching (green line) or a parallel compression (blue line). This result showed that in addition to the "local" effect on individual lipids (in terms of APL, order parameter and membrane thickness) as described above, other effects occurring on larger scales, such as bending, may occur.

Table 2: Area per lipid a, lipid membrane thickness d, and number of hydrogen bonds N_{hd} between water and lipid polar heads derived from MD simulations of small DOPC bilayers at atmospheric pressure (i.e. 0.1 MPa) or under an external and directionnal pressure (along xy or z) of +2.4 MPa (compression) or −2.4 MPa (stretching).

acronym	a (Å^2)	d (Å)	N_{hb}
0.1MPa-xyz	67.5 ± 0.3	42.5 ± 1.0	740 ± 2
0.1MPa-xy_2.4MPa-z	71.9 ± 0.4	39.4 ± 0.7	757 ± 3
0.1MPa-xy_-2.4MPa-z	63.2 ± 0.4	44.2 ± 0.5	721 ± 2
2.4MPa-xy_0.1MPa-z	63.5 ± 0.4	44.4 ± 1.1	722 ± 3
-2.4MPa-xy_0.1MPa-z	72.3 ± 0.2	39.6 ± 0.7	758 ± 1

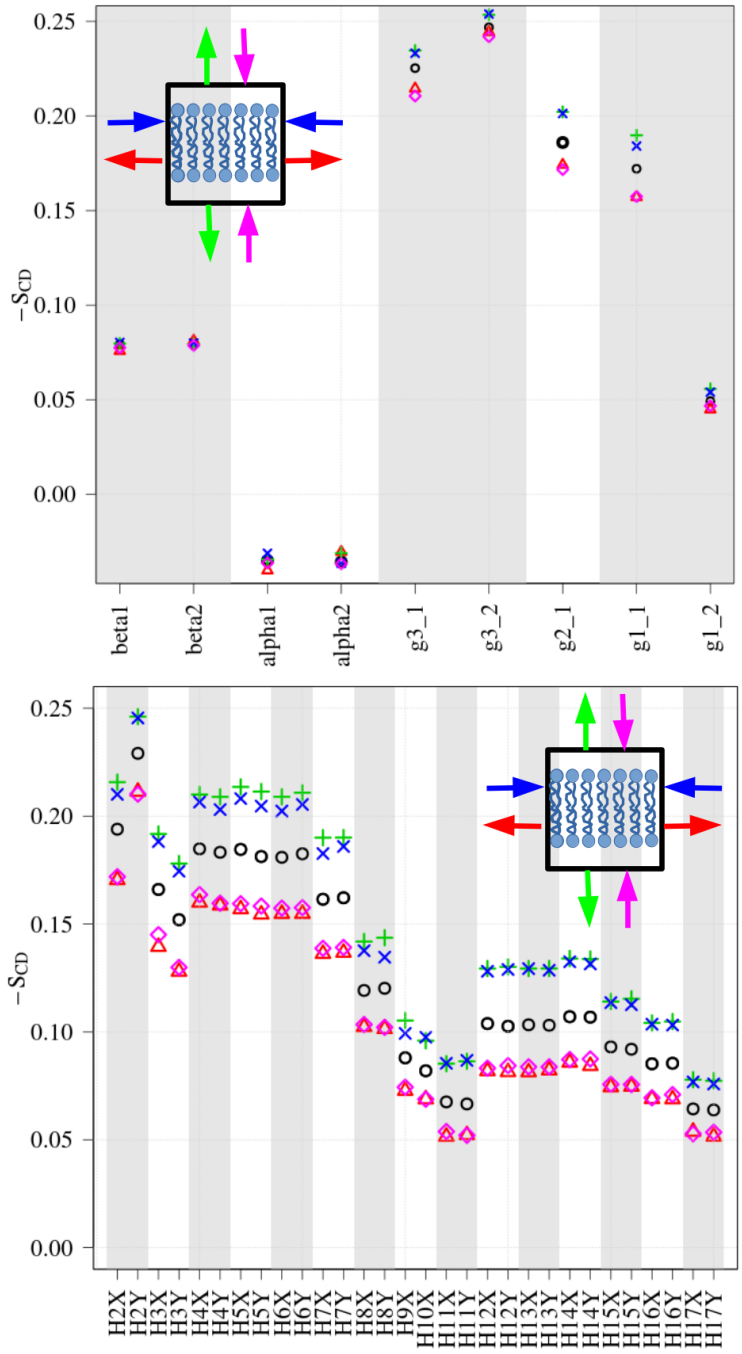

Figure 5: Top panel: Order parameter for each C-H bond of the DOPC polar head. Bottom panel: Order parameter for each C-H bond of the sn-1 DOPC acyl chain. The symbols correspond to the case where a uniform pressure of 0.1 MPa was applied (○), when a pressure of 2.4 MPa (◇) or a -2.4 MPa (+) was applied along z on the box (i.e. perpendicularly to the membrane surface), and when a pressure of 2.4 MPa (×) or -2.4 MPa (△) was applied along xy on the box (i.e. laterally to the membrane). The labels used for each hydrogen name are shown in Fig. 2S. The inset plots recall for each color code how the pressure is applied on the box containing the membrane.

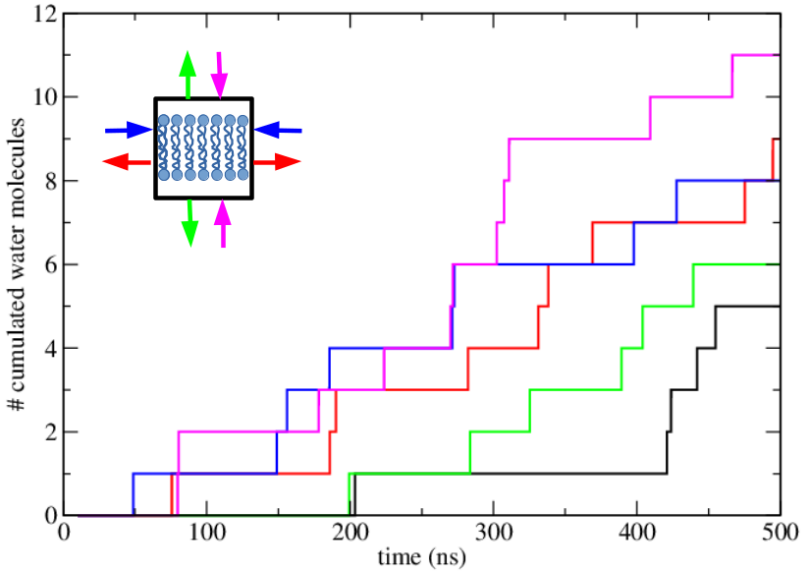

Figure 6: Number of water molecules crossing the DOPC membrane as a function of time. The different lines correspond to the case where a uniform compression of 0.1 MPa was applied in all directions (black), when a pressure of 2.4 MPa (magenta) or of -2.4 MPa (green) was applied along z, and when a pressure of 2.4 MPa (blue) or of -2.4 MPa (red) was applied along xy. The inset plot recalls for each color code how the pressure is applied on the box containing the membrane.

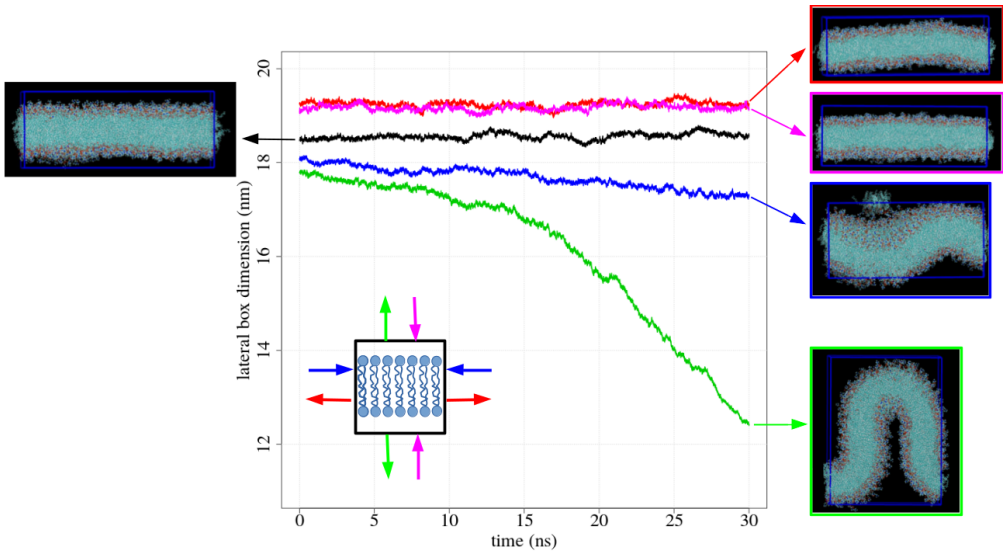

Figure 7: Lateral box size of large DOPC membrane simulations. The lines correspond to the case where a uniform compression of 0.1 MPa was applied in all directions (black), when a pressure of 2.4 MPa (magenta) or of -2.4 MPa (green) was applied along z, and when a pressure of 2.4 MPa (blue) or of -2.4 MPa (red) was applied along xy. The inset plot recalls for each color code how the pressure is applied on the box containing the membrane.

Discussion

Liposome properties and passive release.

DOPC and DSPC exhibit the same chemical structure except that DOPC has a double bond between carbons C9 and C10 for both acyl chains. Because of this unsaturation, the two hydrophobic chains of DOPC form an angle at C9 of about 132°,[39] while they can adopt a straight conformation for DSPC. This leads to differences in the properties of membranes made of DOPC and DSPC such as membrane thickness, area per lipid, hydration or temperature-induced phase transitions. All membranes made of a single lipid type exhibit a gel-to-liquid transition, but the temperature of transition T_m (also called melting temperature) depends of the lipid. In the gel or L_β phase (alternatively called solid ordered or s_o phase in the presence of cholesterol), all fatty chains exhibit a rigid conformation as straight as possible (i.e. the order parameter value is at its highest value) so that the lipids are very tightly packed.[39] In contrast, in the liquid crystalline or L_α phase (alternatively called liquid disordered or l_d phase in the presence of cholesterol), the lipid fatty chains have much more freedom to move (i.e. the order parameter is reduced), the membrane is less packed and the area per lipid is larger.[39] For DSPC, T_m was reported to be 54.5℃,[37] whereas for DOPC the reported values were −16.5, −17.3 or −21℃.[40] Consequently, DOPC membranes remain in a liquid crystalline phase at positive temperatures.

The literature reports an area per lipid of $a = 72.2\,\text{Å}^2$ and a membrane thickness of $d = 35.3\,\text{Å}$ for a DOPC membrane at 30℃.[41] While for a DSPC, the reported values are $a = 47.3\,\text{Å}^2$ and $d = 47\,\text{Å}$[42] at 25℃ when the membrane is in the gel phase and $a = 63.8\,\text{Å}^2$ and $d = 42.2\,\text{Å}$ at 61℃ when the membrane is in the liquid-crystalline phase.[43] Mathai et al.[44] showed that the water permeability of a membrane is correlated to the area per lipid but not to other parameters such as membrane hydrophobic thickness, area compressibility, bending modulus, volume per methyl group or the total lipid volume. Consequently and according to the above literature values of a for DOPC and DSPC, we should expect a

better fluorescein release first, for a DOPC liposome than for a DSPC liposome below T_m and second, for a DSPC liposome above T_m than below T_m. This is indeed what we observed in our experimental data displayed in Fig. 2. For liposomes made purely of DOPC, the passive release over 20 min is always important (over 5%) whatever the temperature and even goes over 50% above 37°C. While for liposomes made purely of DSPC, the passive release is very small ($< 0.1\%$) in the gel phase at 22°C then increases dramatically past the T_m.

The temperature T_m derived from the fit of our data for $\chi_{\text{chol}} = 0$ gives a value of 50.9 ± 0.7°C which is below 54.5°C, the value measured by Ono et al.[37] using differential scanning calorimetry and light scattering (to measure turbidity). Differences between T_m values measured by differential scanning calorimetry and from release experiments were also observed by Ono et al.[37] on dipalmitoylphosphatidylcholine (DPPC) liposomes and by Chen et al.[45] on liposomes made of a mixture of DPPC and hydro soil phosphatidylcholine (HSPC).

The membrane properties (e.g. bending rigidity,[46,47] thickness,[48–50] lipid diffusion[51,52]) are known to vary with the addition of cholesterol or other sterols such as β-sitosterol or stigmasterol.[53] Each of these sterols exhibits a characteristic maximum solubility, χ, in membranes.[54] The maximum mole fraction of cholesterol, χ_{chol}, has been determined in the literature for many types of membrane. Its value is 62 mol%[55] in DOPC membrane, 65-70 mol%[54] in membrane made of DOPC and DPPC, and 66 mol%[56] in membranes made of POPC (16:0-18:1 PC), DEPC (di22:1 PC), DLPC (di12:0 PC), or DPPC (di16:0 PC).

In our measurements, the fraction of cholesterol in DOPC and DSPC liposomes was at most 34 and 44%, respectively, which was below the maximum cholesterol solubility.

In our temperature release experiments displayed in Fig. 2, the first effect observed upon the addition of cholesterol, at a given temperature, is a decrease in fluorescein release for liposomes containing either DOPC or DSPC. This effect could be due to a decrease in the area per lipid upon cholesterol addition.

Indeed, Chakraborty et al.[47] showed that the area per DOPC lipid decreases, at 25°C,

from 61.5 to 48.7 Å^2 when χ_{chol} increases from 0 to 50 mol%. No experimental data was found for DSPC but a similar trend was observed for DMPC (14:0 PC), SOPC (18:0-18:1 PC) and POPC (16:0-18:1 PC).[47,48]

The second effect observed in Fig. 2 due to the addition of cholesterol is a decrease in T_m values when the DSPC membrane contains up to 33 mol% of cholesterol. This behavior is in agreement with literature data performed on liposome membranes made of DNPC[57] (di24:1c15 PC, 1,2-dinervonoyl-sn-glycero-3-phosphocholine), HSPC[58] (Hydrogenated soybean phosphatidylcholine made approximately of 85% DSPC and 15% DPPC), di17:0 PC[59] (1,2-diheptadecanoyl-sn-glycero-3-phosphocholine), DPPC,[11,52,60] and DOPC.[61] This effect can be explained by the fact that the addition of cholesterol rearranges the membrane structure: both L_α and L_β phases are progressively disappearing upon the addition of cholesterol to be progressively replaced by a homogeneous liquid ordered or L_o phase.[60,62] In between, there is a coexistence of membrane regions in the L_o phase with other membrane regions in either L_α or L_β phases, until there is enough cholesterol to create a L_o phase over the whole membrane area. Finally, because L_β and L_o phases are better organized than L_α phase, they also exhibit a better packing. In drug delivery investigations, saturated lipids are favored because of their gel-to-liquid transition and of their low release below T_m. Our results show that there is no advantage of adding cholesterol in liposomes made of a saturated lipid like DSPC as it may dramatically reduce the amount of released drugs. These measurements represent control experiments, measuring the passive release (i.e. in the absence of insonation), that are used to evaluate the enhanced release due to insonation.

Ultrasound-triggered release

Echography uses ultrasound frequencies ranging from 1 to 15 MHz, while for therapeutic applications frequency ranges from 400 kHz to several megahertz. Higher frequencies allow for a smaller focus and hence precision, while lower frequencies allow for a deeper penetration in tissues or through the skull. Thus, the three frequencies used here (0.8, 1.1 and 3.3 MHz)

are relevant for both diagnostic and therapeutic applications. The use of a duty cycle of 5% avoids bringing too much energy at the acoustic focus and hence overheating the focal region. The combination of frequency, pressure and duty cycle values used in our experiments does not lead to inertial cavitation (as measured by the terephtalate dosimeter) and the temperature rise was always contained and never exceeded 2.1℃. It is also informative to calculate the Mechanical Index, defined as MI $= \frac{\mathrm{PNP}}{\sqrt{f}}$, where PNP is the peak negative acoustic pressure. In echography, a MI value higher than 1.9 is prohibited, but a higher value can be used for therapeutic applications such as sono-ablation. In our case, insonation at $f = 0.8\,\mathrm{MHz}$ and $P_{pkpk} = 8\,\mathrm{MPa}$ gives a MI value of 4.5. At $f = 1.1\,\mathrm{MHz}$, the values are 0.95, 1.19 and 2.38 for $P_{pkpk} = 2$, 2.5 and 5 MPa respectively. Finally, MI = 0.55 for $f = 3.3\,\mathrm{MHz}$ and $P_{pkpk} = 2\,\mathrm{MPa}$.

Our experimental data shows that an insonation better enhances the release of fluorescein encapsulated into a DOPC liposomes than in DSPC liposomes. In the absence of cholesterol, the enhancement difference is more than 20 times between DOPC and DSPC liposomes at 37℃. At this temperature, the membrane of DSPC liposomes remains in the gel or solid ordered phase since the elevation of temperature due to the insonation is not enough to go over T_m, even if this value slightly decreases upon the addition of cholesterol (see inset in Fig. 2). The difference in release enhancement becomes small when comparing DSPC formulations and a DOPC liposomes containing 34% of cholesterol. Our data shows that ultrasound is more efficient at enhancing the permeability of a membrane in a liquid crystalline or disordered phase than in a gel or liquid ordered phase. Moreover, we do not see differences due to frequency when comparing release measurements performed at 1.1 or 3.3 MHz. Experiments made at 1.1 MHz indicate a linear dependence on acoustic pressure up to 5 MPa. But this may not be true for higher pressures which can explain the smaller ΔR values measured at 0.8 MHz where experiments were performed a $P_{pkpk} = 8\,\mathrm{MPa}$.

We used a low duty cycle of 5% to reduce heat deposition due to ultrasound. Consequently, during the 20 min insonation ultrasound were effectively "on" only for a cumulated

time of 1 min. Taking this fact into account, our results are in line with Oerlemans et al.[7] who studied the release of fluorescein encapsulated into liposomes made of DSPC, cholesterol and DSPE-PEG_{2000} in a molar ratio of 56:39:5. The authors measured a 5% of release due to a 4 min insonation with $f = 1.5\,\mathrm{MHz}$, $DC = 100\%$ and $P_{pkpk} = 3.2\,\mathrm{MPa}$. While we measured a release value of 2.5% at $P_{pkpk} = 2.5\,\mathrm{MPa}$, $f = 1.1\,\mathrm{MPa}$ and $\chi_{\mathrm{chol}} = 44\,\mathrm{mol\%}$, knowing that a 20 min insonation at $DC = 5\%$ would correspond to 1 min at $DC = 100\%$.

The fact that an unsaturated lipid (i.e. DOPC or DOPE) is better permeabilized under the action of ultrasound than a saturated one (i.e. DSPC) also agrees with the study of Evjen et al.[9] who used doxorubicin encapsulated into liposomes made of 40 mol% of cholesterol and of different ratio of DOPE, DSPC and DSPE-PEG_{2000} (the latter being kept at 8 mol%). The authors obtained the highest release in the absence of DSPC and the lower release at the highest concentration of DSPC after a 6 min insonation performed at a 100% DC, a frequency of 40 kHz, and peak-to-peak pressure of 240 kPa.

If we wish to increase the amount of released drug, one can simply increase the insonation time and/or the duty cycle. This has been demonstrated by Mujoo et al.[12] who showed that the release of carboxyfluorescein encapsulated in DSPC liposomes (with $\chi_{\mathrm{chol}} = 13\,\mathrm{mol\%}$) increases from 0.5% to 5.5% when the insonation time increased from 1 min to 10 min (at $f = 1.1$ MHz, DC = 100%, the authors did not measure the acoustic pressure). In addition, Novell et al.[11] measured a linear increase in the release of calcein encapsulated into liposome made of DPPC (with 30% cholesterol and 5% DPSC-PEG_{2000}) from 4% release upon 5 min insonation ($f = 1\,\mathrm{MHz}$, DC = 40% and PNP = 1.5 MPa) up to 13% release for 30 min insonation.

In our experiments we did not add DSPE-PEG_{2000} into our liposomes, while all of the cited literature studies used a DSPE-PEG_{2000} concentration varying from 5 to 8%. In these investigations, the presence of DSPE-PEG_{2000} aims at reducing the liposome uptake by macrophages. Two studies[45,63] demonstrated that the presence of DSPE-PEG_{2000} modifies the membrane permeability and that the passive[45] or ultrasound triggered[63] release is most

enhanced at concentration varying from 4 to 8%, where DSPE-PEG_{2000} conformation is in a brush regime.

It is worth noting that the results of Giustetto et al.[10] dramatically differ from other studies including ours, as the authors measured an impressive 90% release of gadoteridol (a molecule used as MRI contrast agent) encapsulated into liposome made of DSPC and DSPC-PEG2000 (95:5) after a 5 min insonation at a 100% DC, $f = 28\,\text{kHz}$, $P_{pkpk} = 0.42\,\text{MPa}$, and at room temperature. Since the ultrasonic properties of Giustetto et al. are close to the ones of Evjen et al., the huge difference observed in release is most probably correlated to the difference in the chemical nature of the encapsulated molecules.

Overall, our experimental data confirmed that an insonation leads to an enhancement in the release of fluorescein from liposomes in the absence of cavitation and below T_m in the case of DSPC liposomal formulation. Our data indicates that ultrasound is more efficient to increase release for liposomes made of unsaturated lipids and this effect is more pronounced in the absence of cholesterol. Since Mathai et al.[44] experimentally determined that membrane permeability mainly depends on the area per lipid, we can expect that the action of an acoustic pressure lies in the modification of this parameter.

MD simulations of DOPC membranes under a directional pressure

In all our small patch simulations, we only observe crossing events of individual water molecules, no pore or hole is present. Therefore, each crossing water is surrounded by a spherical "cage" of methylenes (or methyls) whose size minimizes their mutual contact surface. Each crossing event is fairly fast, occurring on a few ns time scale. The free energy of water crossing using CHARMM36 force field has been evaluated around 25–27 kJ/mol in DPPC at 49.85℃.[64] Here we have a DOPC bilayer at 22℃. Although the exact free energy barrier value is probably different due to the conditions and lipid composition, we expect it to be on the same order of magnitude for the reference simulation at 0.1 MPa. This range of barrier value makes water crossing a rather rare event, on the order of 1 water molecule

per 100 ns for 100 lipids. Interestingly, for three of the simulations under high pressure, this free energy is lowered since we observe more permeation events. At the conditions for which the APL increases (lateral stretching (red curves) and perpendicular compression (magenta curves)), this result is logical since this APL increase should make more space for water to enter the bilayer. For the lateral compression (blue curves), there is a drop in APL accompanied with a rise of water molecules crossing the membrane. This result is counter-intuitive. Tightly packed lipids could be thought to be less permeable to water compared to a membrane at rest. It remains unclear why we observe this phenomenon.

Simulations on large patches show that the membrane experiences large deformations under lateral compression or perpendicular stretching, such as membrane buckling. This is important to keep in mind that imposing periodic boundary conditions (PBC) on the membrane, as is routinely used in all-atom membrane simulations, imposes an artificial ordering. The edges of the membrane remain connected through the PBC. Instead, in real life we deal with spherical liposomes which probably change their shape during insonation. We expect them to pass from a sphere to an ellipsoid. Thus, we do not think that what we observe in our large membrane simulations occurs exactly in the same manner in real life, but rather we want to stress that bending is one type of response to alleviate the pressure felt by the membrane in case of lateral compression or perpendicular stretching. Thus, we cannot rule out that a change in liposome shape could also come with high curvature membrane bending. Interestingly, a recent study showed that positive (convex) and negative (concave) curvature increases water permeability on an asymmetric composition mimicking the plasma membrane.[65] Positive curvature implies that the polar heads get further apart which creates packing defects[66] facilitating water entry into the membrane. For negative curvature, it is less clear why water permeability is enhanced compared to a flat membrane.

Overall, our MD simulations show that the application of a directional pressure modifies the membrane properties and enhances the membrane permeability to water. Consequently, we can expect the same effect to happen with an acoustic pressure in our experiments with

fluorescein-loaded liposomes. This suggests that the triggered release of fluorescein in our experiments is most probably due to an enhanced diffusion of fluorescein out of the liposome thanks to a higher membrane permeability.

To obtain a complementary view of the mechanism at play in our experiments, several systems could be simulated.

First, it will be important to simulate a whole liposome. The simulation of a liposome of 100 nm of diameter is now possible using coarse-grained simulations with current hardware and softwares. However, this is at the cost of loosing valuable atomic information about membrane permeability. Simulating a whole liposome could be especially interesting for understanding how it changes its shape under the applied pressures. As hypothesized above, it remains especially unknown whether this change of shape is accompanied by some large undulations or local buckling.

Secondly, it would be interesting to use a sinusoidal pressure variation. So far, the group of Nguyen has successfully implemented this possibility[23,67] but on a rather old version of GROMACS (i.e. 5.0.7). In their paper, they studied in particular the effect of a focused ultrasound (at $f = 10\,\mathrm{MHz}$ and $P_{pkpk} = 11\,\mathrm{MPa}$) on a circular region of 10 nm of diameter of a rectangular DOPC membrane of $40\,\mathrm{nm}^2$.[67] The region outside of the circular region not being submitted to the sinusoidal pressure variation. The formation of a hole into the membrane was observed in their simulations. This study was interesting for understanding how the applied pressure dissipates the energy on the neighboring lipids out of the focused ultrasound. However, such a small focal section is experimentally unreachable using clinically relevant frequencies. For instance, in our case the smallest diameter of the focal section is 620 µm when $f = 3.3\,\mathrm{MHz}$. Moreover, in our case, we wanted to focus on pressures that are one order of magnitude below theirs to avoid important damages on the membrane.

Thirdly, it would also be interesting to test the release of some embedded molecules within the liposomes (fluorescein or other small molecules alike) using coarse-grained simulations.

Conclusion

Our results show that a moderate acoustic pressure induces fluorescein release for all formulations but at different degrees. The highest ultrasound-triggered release is obtained for a liposome made of pure DOPC membrane, but passive release is also important. The lowest ultrasound-triggered release is measured for DSPC liposomes which also exhibit a very small passive release. The fluorescein release is not due to inertial cavitation or heating but to an enhanced diffusion of fluorescein out of the liposome, partially due to an increase in area per lipid as suggested by our MD simulations. This enhanced release diffusion mechanism requires insonations of several minutes but does not require high pressures, so a low mechanical index could be used.

Acknowledgement

F. E.-H. acknowledges the financial support of her Ph.D by AUF / CNRS-L / UL.

Supporting Information Available

The following files are available free of charge.

- Figure 1S: Order parameter, S_{CD}, derived from all simulations for the second fatty chain of DOPC lipid (see Fig. 5 for the first chain),
- Figure 2S: DOPC structure displaying the atom labels used in the figures plotting the order parameters,
- Figure 3S: Areas per DOPC lipid, a, derived from all simulations,
- Figure 4S: Membrane thickness, d, derived from all simulations,
- Figure 5S: Number of hydrogen bonds, N_{hb}, between DOPC polar head and water derived from all simulations.

- Figure 6S: Heatmap of p-values that indicates if the points displayed in the top figure of Fig. 3 are significantly different.
- Figure 7S: Heatmap of p-values that indicates if the points displayed in the bottom figure of Fig. 3 are significantly different.
- Figure 8S: Heatmap of p-values that indicates if the points displayed in the top figure of Fig. 4 are significantly different.
- Figure 9S: Heatmap of p-values that indicates if the points displayed in the bottom figure of Fig. 4 are significantly different.
- Figure 10S: Power spectrum densities of acoustic signals measured at the transducer focus by a needle hydrophone in the absence of liposomes.

References

(1) Immordino, M. L.; Dosio, F.; Cattel, L. Stealth liposomes: review of the basic science, rationale, and clinical applications, existing and potential. Int. J. Nanomed. **2006**, 1, 297.

(2) Gabizon, A. A. Pegylated Liposomal Doxorubicin: Metamorphosis of an Old Drug into a New Form of Chemotherapy. Cancer Invest. **2001**, 19, 424–436.

(3) Maruyama, K.; Ishida, O.; Takizawa, T.; Moribe, K. Possibility of active targeting to tumor tissues with liposomes. Adv. Drug Deliv. Rev. **1999**, 40, 89–102.

(4) Kaur, I. P.; Garg, A.; Singla, A. K.; Aggarwal, D. Vesicular systems in ocular drug delivery: an overview. Int. J. Pharm. **2004**, 269, 1–14.

(5) Lyon, P. C.; Griffiths, L. F.; Lee, J.; Chung, D.; Carlisle, R.; Wu, F.; Middleton, M. R.; Gleeson, F. V.; Coussios, C. C. Clinical trial protocol for TARDOX: a phase I study

to investigate the feasibility of targeted release of lyso-thermosensitive liposomal doxorubicin (ThermoDox®) using focused ultrasound in patients with liver tumours. J. Ther. Ultrasound **2017**, 5, 28.

(6) Afadzi, M.; Davies, C. d. L.; Hansen, Y. H.; Johansen, T.; Standal, Ø. K.; Hansen, R.; Måsøy, S.-E.; Nilssen, E. A.; Angelsen, B. Effect of ultrasound parameters on the release of liposomal calcein. Ultrasound Med. Biol. **2012**, 38, 476–486.

(7) Oerlemans, C.; Deckers, R.; Storm, G.; Hennink, W. E.; Nijsen, J. F. W. Evidence for a new mechanism behind HIFU-triggered release from liposomes. J. Control. Release **2013**, 168, 327–333.

(8) Evjen, T. J.; Nilssen, E. A.; Rögnvaldsson, S.; Brandl, M.; Fossheim, S. L. Distearoylphosphatidylethanolamine-based liposomes for ultrasound-mediated drug delivery. Eur. J. Pharm. Biopharm. **2010**, 75, 327–333.

(9) Evjen, T. J.; Hagtvet, E.; Nilssen, E. A.; Brandl, M.; Fossheim, S. L. Sonosensitive dioleoylphosphatidylethanolamine-containing liposomes with prolonged blood circulation time of doxorubicin. Eur. J. Pharm. Sci. **2011**, 43, 318–324.

(10) Giustetto, P.; Castelli, D. D.; Boffa, C.; Rizzitelli, S.; Durando, D.; Cutrin, J. C.; Aime, S.; Terreno, E. Release of a paramagnetic magnetic resonance imaging agent from liposomes triggered by low intensity non-focused ultrasound. J. Med. Imaging Health Inform. **2013**, 3, 356–366.

(11) Novell, A.; Sabbagh, C. A.; Escoffre, J.-M.; Gaillard, C.; Tsapis, N.; Fattal, E.; Bouakaz, A. Focused ultrasound influence on calcein-loaded thermosensitive stealth liposomes. Int. J. Hyperthermia **2015**, 31, 349–358.

(12) Mujoo, H.; Reynolds, J. N. J.; Tucker, I. G. The influence of bile salts on the response of liposomes to ultrasound. J. Liposome Res. **2016**, 26, 87–95.

(13) Verchère, A.; Dezi, M.; Broutin, I.; Picard, M. In vitro investigation of the MexAB efflux pump from Pseudomonas aeruginosa. J. Vis. Exp. **2014**, e50894.

(14) Grohganz, H.; Ziroli, V.; Massing, U.; Brandl, M. Quantification of various phosphatidylcholines in liposomes by enzymatic assay. Aaps Pharmscitech **2003**, 4, 500–505.

(15) Mailer, A. G.; Clegg, P. S.; Pusey, P. N. Particle sizing by dynamic light scattering: non-linear cumulant analysis. J. Phys. Condens. Matter **2015**, 27, 145102.

(16) Iida, Y.; Yasui, K.; Tuziuti, T.; Sivakumar, M. Sonochemistry and its dosimetry. Microchem. J. **2005**, 80, 159–164.

(17) McLean, J.; Mortimer, A. A cavitation and free radical dosimeter for ultrasound. Ultrasound Med. Biol. **1988**, 14, 59–64.

(18) Price, G. J.; Duck, F. A.; Digby, M.; Holland, W.; Berryman, T. Measurement of radical production as a result of cavitation in medical ultrasound fields. Ultrason. Sonochem. **1997**, 4, 165–171.

(19) Somaglino, L.; Bouchoux, G.; Mestas, J.-L.; Lafon, C. Validation of an acoustic cavitation dose with hydroxyl radical production generated by inertial cavitation in pulsed mode: Application to in vitro drug release from liposomes. Ultrason. Sonochem. **2011**, 18, 577–588.

(20) Rifai, N. A.; Desgranges, S.; Guillou-Buffello, D. L.; Giron, A.; Urbach, W.; Nassereddine, M.; Charara, J.; Contino-Pépin, C.; Taulier, N. Ultrasound-triggered delivery of paclitaxel encapsulated in an emulsion at low acoustic pressures. J. Mater. Chem. B **2020**, 8, 1640–1648.

(21) Jo, S.; Kim, T.; Iyeryashankara, V. G.; Im, W. CHARMM-GUI: A web-based graphical user interface for CHARMM. J. Comput. Chem. **2008**, 29, 1859–1865.

(22) Koshiyama, K.-i.; Kodama, T.; Yano, T.; Fujikawa, S. Molecular dynamics simulation of water pore formation in lipid bilayer induced by shock waves. AIP Conference Proceedings. 2006; pp 583–587.

(23) Man, V. H.; Li, M. S.; Derreumaux, P.; Wang, J.; Nguyen, T. T.; Nangia, S.; Nguyen, P. H. Molecular mechanism of ultrasound interaction with a blood brain barrier model. J. Chem. Phys. **2020**, 153, 045104.

(24) Klauda, J. B.; Venable, R. M.; Freites, J. A.; O'Connor, J. W.; Tobias, D. J.; Mondragon-Ramirez, C.; Vorobyov, I.; MacKerell, A. D.; Pastor, R. W. Update of the CHARMM All-Atom Additive Force Field for Lipids: Validation on Six Lipid Types. J. Phys. Chem. B **2010**, 114, 7830–7843.

(25) Abraham, M. J.; Murtola, T.; Schulz, R.; Páll, S.; Smith, J. C.; Hess, B.; Lindahl, E. GROMACS: High performance molecular simulations through multi-level parallelism from laptops to supercomputers. SoftwareX **2015**, 1–2, 19–25.

(26) Berendsen, H. J. C.; Postma, J. P. M.; van Gunsteren, W. F.; DiNola, A.; Haak, J. R. Molecular dynamics with coupling to an external bath. J. Chem. Phys. **1984**, 81, 3684–3690.

(27) Bussi, G.; Donadio, D.; Parrinello, M. Canonical sampling through velocity rescaling. J. Chem. Phys. **2007**, 126, 014101.

(28) Parrinello, M.; Rahman, A. Polymorphic transitions in single crystals: A new molecular dynamics method. J. Appl. Phys. **1981**, 52, 7182–7190.

(29) Hess, B. P-LINCS: A Parallel Linear Constraint Solver for Molecular Simulation. J. Chem. Theory Comput. **2008**, 4, 116–122.

(30) Miyamoto, S.; Kollman, P. A. Settle: An analytical version of the SHAKE and RATTLE algorithm for rigid water models. J. Comput. Chem. **1992**, 13, 952–962.

(31) Steinbach, P. J.; Brooks, B. R. New spherical-cutoff methods for long-range forces in macromolecular simulation. J. Comput. Chem. **1994**, 15, 667–683.

(32) Darden, T.; York, D.; Pedersen, L. Particle mesh Ewald: An N log(N) method for Ewald sums in large systems. J. Chem. Phys. **1993**, 98, 10089–10092.

(33) Essmann, U.; Perera, L.; Berkowitz, M. L.; Darden, T.; Lee, H.; Pedersen, L. G. A smooth particle mesh Ewald method. J. Chem. Phys. **1995**, 103, 8577–8593.

(34) Humphrey, W.; Dalke, A.; Schulten, K. VMD: Visual molecular dynamics. J. Mol. Graph. **1996**, 14, 33–38.

(35) Botan, A. et al. Toward Atomistic Resolution Structure of Phosphatidylcholine Headgroup and Glycerol Backbone at Different Ambient Conditions. J. Phys. Chem. B **2015**, 119, 15075–15088.

(36) Melo, M. N.; Arnarez, C.; Sikkema, H.; Kumar, N.; Walko, M.; Berendsen, H. J. C.; Kocer, A.; Marrink, S. J.; Ingólfsson, H. I. High-Throughput Simulations Reveal Membrane-Mediated Effects of Alcohols on MscL Gating. J. Am. Chem. Soc. **2017**, 139, 2664–2671.

(37) Ono, A.; Takeuchi, K.; Sukenari, A.; Suzuki, T.; Adachi, I.; Ueno, M. Reconsideration of drug release from temperature-sensitive liposomes. Biol. Pharm. Bull. **2002**, 25, 97–101.

(38) Nelson, S. C.; Neeley, S. K.; Melonakos, E. D.; Bell, J. D.; Busath, D. D. Fluorescence anisotropy of diphenylhexatriene and its cationic Trimethylamino derivative in liquid dipalmitoylphosphatidylcholine liposomes: opposing responses to isoflurane. BMC Biophys. **2012**, 5.

(39) Jaschonek, S.; Cascella, M.; Gauss, J.; Diezemann, G.; Milano, G. Intramolecular structural parameters are key modulators of the gel-liquid transition in coarse grained simu-

lations of DPPC and DOPC lipid bilayers. Biochem. Biophys. Res. Comm. **2018**, 498, 327–333.

(40) Kaneshina, S.; Ichimori, H.; Hata, T.; Matsuki, H. Barotropic phase transitions of dioleoylphosphatidylcholine and stearoyl-oleoylphosphatidylcholine bilayer membranes. Biochim. Biophys. Acta Biomembr. **1998**, 1374, 1–8.

(41) Tristram-Nagle, S.; Petrache, H. T.; Nagle, J. F. Structure and Interactions of Fully Hydrated Dioleoylphosphatidylcholine Bilayers. Biophys. J. **1998**, 75, 917–925.

(42) Sun, W. J.; Tristram-Nagle, S.; Suter, R. M.; Nagle, J. F. Structure of gel phase saturated lecithin bilayers: temperature and chain length dependence. Biophys. J. **1996**, 71, 885–891.

(43) Kučerka, N.; Nieh, M.-P.; Katsaras, J. Fluid phase lipid areas and bilayer thicknesses of commonly used phosphatidylcholines as a function of temperature. Biochim. Biophys. Acta Biomembr. **2011**, 1808, 2761–2771.

(44) Mathai, J. C.; Tristram-Nagle, S.; Nagle, J. F.; Zeidel, M. L. Structural Determinants of Water Permeability through the Lipid Membrane. J. Gen. Physiol. **2007**, 131, 69–76.

(45) Chen, J.; Cheng, D.; Li, J.; Wang, Y.; Guo, J.-X.; Chen, Z.-P.; Cai, B.-C.; Yang, T. Influence of lipid composition on the phase transition temperature of liposomes composed of both DPPC and HSPC. Drug Dev. Ind. Pharm. **2013**, 39, 197–204.

(46) Silva, C.; Aranda, F. J.; Ortiz, A.; Martínez, V.; Carvajal, M.; Teruel, J. A. Molecular aspects of the interaction between plants sterols and DPPC bilayers: an experimental and theoretical approach. J. Coll. Int. Sci. **2011**, 358, 192–201.

(47) Chakraborty, S.; Doktorova, M.; Molugu, T. R.; Heberle, F. A.; Scott, H. L.; Dzikovski, B.; Nagao, M.; Stingaciu, L.-R.; Standaert, R. F.; Barrera, F. N.; Kat-

saras, J.; Khelashvili, G.; Brown, M. F.; Ashkar, R. How cholesterol stiffens unsaturated lipid membranes. Proc. Natl. Acad. Sci. **2020**, 117, 21896–21905.

(48) Hung, W.-C.; Lee, M.-T.; Chen, F.-Y.; Huang, H. W. The Condensing Effect of Cholesterol in Lipid Bilayers. Biophys. J. **2007**, 92, 3960–3967.

(49) Pan, J.; Tristram-Nagle, S.; Nagle, J. F. Effect of cholesterol on structural and mechanical properties of membranes depends on lipid chain saturation. Phys. Rev. E **2009**, 80, 021931.

(50) Madej, B. D.; Gould, I. R.; Walker, R. C. A Parameterization of Cholesterol for Mixed Lipid Bilayer Simulation within the Amber Lipid14 Force Field. J. Phys. Chem. B **2015**, 119, 12424–12435.

(51) Kahya, N.; Schwille, P. How Phospholipid-Cholesterol Interactions Modulate Lipid Lateral Diffusion, as Revealed by Fluorescence Correlation Spectroscopy. J. Fluoresc. **2006**, 16, 671–678.

(52) Jovanović, A. A.; Balanč, B. D.; Ota, A.; Grabnar, P. A.; Djordjević, V. B.; Šavikin, K. P.; Bugarski, B. M.; Nedović, V. A.; Ulrih, N. P. Comparative Effects of Cholesterol and β-Sitosterol on the Liposome Membrane Characteristics. Eur. J. Lipid Sci. Technol. **2018**, 120, 1800039.

(53) Demel, R.; De Kruyff, B. The function of sterols in membranes. Biochim. Biophys. Acta Biomembr. **1976**, 457, 109–132.

(54) Stevens, M. M.; Honerkamp-Smith, A. R.; Keller, S. L. Solubility limits of cholesterol, lanosterol, ergosterol, stigmasterol, and β-sitosterol in electroformed lipid vesicles. Soft Matter **2010**, 6, 5882–5890.

(55) Parker, A.; Miles, K.; Cheng, K. H.; Huang, J. Lateral Distribution of Cholesterol in

Dioleoylphosphatidylcholine Lipid Bilayers: Cholesterol-Phospholipid Interactions at High Cholesterol Limit. Biophys. J. **2004**, 86.

(56) Huang, J.; Buboltz, J. T.; Feigenson, G. W. Maximum solubility of cholesterol in phosphatidylcholine and phosphatidylethanolamine bilayers. Biochim. Biophys. Acta Biomembr. **1999**, 1417, 89–100.

(57) Gallová, J.; Klacsová, M.; Devínsky, F.; Balgavý, P. Partial volumes of cholesterol and monounsaturated diacylphosphatidylcholines in mixed bilayers. Chem. Phys. Lipids **2015**, 190, 1–8.

(58) Kitayama, H.; Takechi, Y.; Tamai, N.; Matsuki, H.; Yomota, C.; Saito, H. Thermotropic Phase Behavior of Hydrogenated Soybean Phosphatidylcholine–Cholesterol Binary Liposome Membrane. Chem. Pharm. Bull. **2014**, 62, 58–63.

(59) Tamai, N.; Uemura, M.; Goto, M.; Matsuki, H.; Kaneshina, S. Lateral phase separation in cholesterol/diheptadecanoylphosphatidylcholine binary bilayer membrane. Coll. Surf. B **2008**, 65, 213–219.

(60) Redondo-Morata, L.; Giannotti, M. I.; Sanz, F. Influence of Cholesterol on the Phase Transition of Lipid Bilayers: A Temperature-Controlled Force Spectroscopy Study. Langmuir **2012**, 28, 12851–12860.

(61) Fritzsching, K. J.; Kim, J.; Holland, G. P. Probing lipid–cholesterol interactions in DOPC/eSM/Chol and DOPC/DPPC/Chol model lipid rafts with DSC and ^{13}C solid-state NMR. Biochim. Biophys. Acta Biomembr. **2013**, 1828, 1889–1898.

(62) de Meyer, F.; Smit, B. Effect of cholesterol on the structure of a phospholipid bilayer. Proc. Nat. Acad. Sci. USA **2009**, 106, 3654–3658.

(63) Lin, H.-Y.; Thomas, J. L. PEG-Lipids and Oligo(ethylene glycol) Surfactants Enhance the Ultrasonic Permeabilizability of Liposomes. Langmuir **2003**, 19, 1098–1105.

(64) Awoonor-Williams, E.; Rowley, C. N. Molecular simulation of nonfacilitated membrane permeation. Biochim. Biophys. Acta Biomembr. **2016**, 1858, 1672–1687.

(65) Yesylevskyy, S.; Rivel, T.; Ramseyer, C. Curvature increases permeability of the plasma membrane for ions, water and the anti-cancer drugs cisplatin and gemcitabine. Sci. Rep. **2019**, 9, 17214.

(66) Vanni, S.; Hirose, H.; Barelli, H.; Antonny, B.; Gautier, R. A sub-nanometre view of how membrane curvature and composition modulate lipid packing and protein recruitment. Nature Comm. **2014**, 5, 4916.

(67) Man, V. H.; Li, M. S.; Wang, J.; Derreumaux, P.; Nguyen, P. H. Interaction mechanism between the focused ultrasound and lipid membrane at the molecular level. J. Chem. Phys. **2019**, 150, 215101.

Graphical TOC Entry